

Zweitveröffentlichung/ Secondary Publication



Staats- und
Universitätsbibliothek
Bremen

<https://media.suub.uni-bremen.de>

Yang Li, Peng Xiao, Yuan Shi, Renato S. M. Almeida, Wei Zhou, Zhuan Li, Heng Luo, Florian Reichert, Nico Langhof, Walter Krenkel

[+]

Mechanical behavior of LSI based C/C-SiC composites subjected to flexural loadings

Journal Article as: peer-reviewed accepted version (Postprint)

DOI of this document*(secondary publication): 10.26092/elib/2604

Publication date of this document: 24/10/2023

* for better findability or for reliable citation

Recommended Citation (primary publication/Version of Record) incl. DOI:

Yang Li, Peng Xiao, Yuan Shi, Renato S.M. Almeida, Wei Zhou, Zhuan Li, Heng Luo, Florian Reichert, Nico Langhof, Walter Krenkel,

Mechanical behavior of LSI based C/C-SiC composites subjected to flexural loadings,
Composites Part A: Applied Science and Manufacturing, Volume 95, 2017, Pages 315-324, ISSN 1359-835X,
<https://doi.org/10.1016/j.compositesa.2017.01.024>

Please note that the version of this document may differ from the final published version (Version of Record/primary publication) in terms of copy-editing, pagination, publication date and DOI. Please cite the version that you actually used. Before citing, you are also advised to check the publisher's website for any subsequent corrections or retractions (see also <https://retractionwatch.com/>).

This document is made available under a Creative Commons licence.

The license information is available online: <https://creativecommons.org/licenses/by-nc-nd/4.0/>

Take down policy

If you believe that this document or any material on this site infringes copyright, please contact publizieren@suub.uni-bremen.de with full details and we will remove access to the material.

Mechanical behavior of LSI based C/C-SiC composites subjected to flexural loadings

Yang Li^{a,b}, Peng Xiao^{a,*}, Yuan Shi^c, Renato S.M. Almeida^d, Wei Zhou^{a,*}, Zhuan Li^{a,*}, Heng Luo^a, Florian Reichert^b, Nico Langhof^b, Walter Krenkel^b

^a State Key Laboratory of Powder Metallurgy, Central South University, Changsha 410083, PR China

^b Ceramic Materials Engineering, University of Bayreuth, Bayreuth 95447, Germany

^c Institute of Structures and Design, German Aerospace Center, Stuttgart 70569, Germany

^d Advanced Ceramics, University of Bremen, Bremen 28359, Germany

ABSTRACT

Keywords:

C/C-SiC

Flexural fatigue

Interfacial degradation

3D reinforcement

In general, flexural loads result in more complicated and uneven stress distributions in specimens, compared to axial loading. This study reports the influence of flexural fatigue loads including different stress levels and cycles on the mechanical behavior of a 3D C/C-SiC composite. The cyclic tensile loads in the lower part of the specimens result in strength enhancement after short fatigue duration with the expense of decreased flexural modulus due to the fatigue damage such as cracking and interfacial degradation. Whereas the upper part of the post-fatigue specimens, which is almost free of fatigue damage under compressive stress, can still properly deflect the cracks and result in quasi-plastic failures like virgin specimens. Most notably, specimens will suffer strength decline rapidly, after 50,000 cycles with maximum stress of 95 MPa for instance, because of considerable stress concentrations and wear of fibers at 90° fiber bundles in the lower part.

1. Introduction

Since the 1990s, liquid silicon infiltration (LSI) based ceramic matrix composites (CMCs) have been well developed with advantages of moderate costs and suitable efficiency [1,2]. In order to manufacture C/C-SiC with desirable physical properties, a variety of porous C/C based on different carbon precursors including polymers (e.g. resin) and gases (e.g. C₃H₆) were applied [3,4]. Currently, such C/C-SiC composites have already been successfully applied in space structures or high performance braking systems, etc. [5,6]. As an important member of the LSI based C/C-SiC family, the C/C-SiC composites reinforced by 3 dimensional (3D) carbon fibers preform with chemical vapor infiltration (CVI) derived carbon matrix, show excellent physical properties like favorable fracture toughness, and suitable coefficient of friction for different tribological applications [7–9]. So far, the extensive interests concerning 3D carbon fiber preform reinforced C/C-SiC composite (3D C/C-SiC) were mainly focused on low cost manufacturing routes and improvements for mechanical or tribological performance, etc. [10–15]. However,

only a few investigations are centered on the mechanical behavior of the 3D C/C-SiC composite under dynamic loads. Generally, the dynamic loads can lead to mechanical degradation or enhancement during the lifetime of a CMCs component [16–18]. Moreover, the mechanisms of CMCs subjected to fatigue loadings and their mechanical responses, e.g. fracture behavior, are rather complex. Thus, it is quite essential to get fully understanding for the mechanical performance under fatigue loadings. Nowadays, numerous tensile fatigue tests with various test parameters including frequencies, stress levels, stress ratios, etc., are widely developed and applied to characterize the fatigue behavior of CMCs with some nondestructive examinations [19–24]. The studies concerning the fatigue behavior for the CMCs in the last decades indicated that the CMCs show high fatigue limits and the interfacial variation, crack multiplication as well as released thermal residual stress, etc., could enhance the residual strength under tensile fatigue stress [16,25]. In this matter, our previous work regarding the tensile fatigue behavior of a 3D C/C-SiC composites, indicated that such composite shows a high fatigue limit (approximately 75% of the ultimate tensile strength), and the cyclic tensile loading still enhances the material strength, even after one million of cycles [26].

* Corresponding authors.

E-mail addresses: xiaopengcsu@csu.edu.cn (P. Xiao), chowwy@163.com (W. Zhou), lizhuan@csu.edu.cn (Z. Li).

However, components which are made of CMCs are frequently subjected to different types of loadings besides pure tensile or compressive stress. In tribological applications for instance, bending loads could be generated. In this case, the previous works on the axial fatigue behavior are factually insufficient to assess the mechanical responses of CMCs under dynamic flexural loadings due to the totally different stress distributions in off-axial loading. Generally, the strain distributions across the specimens subjected to the tensile-tensile or tensile-compressive cyclic loads are nearly uniform, and the damage induced by the tensile fatigue loads could be more or less identical within each layer of the composite [27,28]. Whereas, the unevenly distributed stresses, e.g. compressive and tensile stresses, will simultaneously occur in the specimen under flexural loading, which could lead to a different mechanical response, e.g. gradiently increased strain distribution and damage at the tensile side and almost free of damage in compressive side of the specimens [27,29]. Therefore, the cyclic flexural tests have been gradually developed in order to perform comprehensive studies on the mechanical behavior for some of CMCs, especially for C/C composites. According to previous work [30–32], the cyclical flexural tests could also yield many useful information, hysteresis behavior and decreased flexural modulus in C/C composites for instance, and be of an effective approach to characterize fatigue properties for some of CMCs with pyrolytic carbon (PyC) interface. Hence, the topic of this work is to investigate the mechanical behavior of a 3D C/C-SiC composite subjected to quasi-static and dynamic flexural loadings. In addition, it is addressed the relationship between the flexural modulus (FM), residual flexural strength (RFS) and permanent strain (PS) with the number of fatigue cycles and fatigue stresses. The microstructures and fractured surfaces of composites with and without previous fatigue loadings were also characterized by optical microscope (OM) and scanning electron microscope (SEM) for examining the fatigue induced damages.

2. Materials and experimental procedures

2.1. Preparation of the C/C-SiC composites

The fabrication process of the composites mainly consists of three steps, as shown in Fig. 1. The Polyacrylonitrile (PAN) based carbon fibers (Toray T700, filament of 12 K) were used as reinforcements for the commercially available 3D fiber preform. Firstly, the chopped fiber web and unidirectional fiber cloth were repeatedly stacked and then needle-punched. The bulk density of 3D fiber preform was of about $0.65 \text{ g} \cdot \text{cm}^{-3}$. Afterwards, a chemical vapor infiltration (CVI) process was performed at 1000°C in argon with an absolute pressure of 0.1 MPa to consolidate the porous C/C composites. Finally, the LSI process was applied to infiltrate the

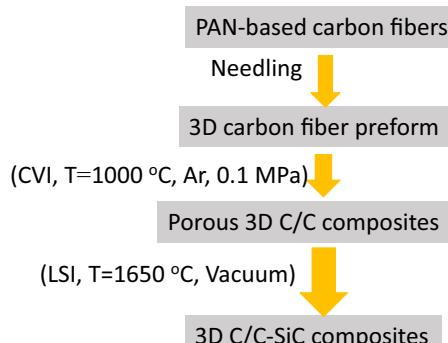


Fig. 1. Schematic illustration of the manufacturing process for the 3D C/C-SiC composites. (For interpretation of the references to color in this figure legend, the reader is referred to the web version of this article.)

above-mentioned porous C/C material. Silicon powder with particle size of approximately $50 \mu\text{m}$ and purity of 99.0% was used for the LSI process. The infiltration in this work was conducted at 1650°C with 0.5 h dwell time under vacuum. More details concerning the preparation of the 3D C/C-SiC was reported previously [7].

2.2. Experimental procedures

All specimens were cut from bulk C/C-SiC composites by using a diamond saw. In addition, samples were grinded and polished to adjust the cross-sections. The open porosity and bulk density of the as-prepared C/C-SiC composites were measured by Archimedes method in distilled water. All 3 point flexural tests were carried out on an universal testing machine (Hegewald & Perchke Inspect table 5 KN) with $55 \times 10 \times 4 \text{ mm}^3$ specimens, as shown in Fig. 2. In order to obtain sufficient specimens from the composites plates for the tests, in this work a span-to-thickness ratio of 10 was used. Note that the ratio of 10 also has been widely used for dynamic or quasi-static flexural tests of CMCs in previous publications [32–36]. Furthermore, the loading rate for the quasi-static flexural test was set to 1 mm/min . According to the standard DIN 658-3, the nominal bending strength (σ) was then calculated using the Eq. (2.1).

$$\sigma = \frac{3FL}{2bd^2} \quad (2.1)$$

where F is the applied force, L is the distance between the rolls, b is the width of specimens, and d is the thickness of specimens.

The flexural fatigue tests were performed by using a sine-wave loading with frequency of 1 Hz and a stress ratio of 0.1 . In addition, the flexural fatigue experiments were monitored by recording of the associated stress-strain curve. The strain was measured by the cross-head travel distance. Regarding the flexural fatigue loading, three sets of tests with different parameters were realized, as shown in Table 1. In the Set 1, the specimens were subjected to different stresses ranging from 180 MPa to 95 MPa in order to define the low-cycles fatigue limit. Note that the flexural specimens were cyclically loaded until total failure or until the run-out was achieved. The run-out in this work was defined as 5×10^4 cycles due to self-limitations from the test machine. In order to study the influence of the fatigue stress on the residual flexural strength after fatigue loadings, tests of 2000 cycles were performed, corresponding to "Set 2". Furthermore, the dependence of RFS on the number of previous fatigue cycles applied was studied with the fatigue stress of 95 MPa during "Set 3".

After fatigue tests, the post-fatigue specimens were quasi-statically loaded until failure in order to determine the residual flexural strength, following the aforementioned procedure for quasi-static flexural tests. Finally, the microstructures and fractured surfaces of the C/C-SiC composites before and after fatigue loadings were analyzed under an optical microscope (AxioTech HAL100, Zeiss) and a scanning electron microscope (SEM, JEOL JSM 6400).

3. Results and discussion

3.1. Weibull distribution of the flexural strength

The general properties of the as-prepared 3D C/C-SiC composites before flexural fatigue loading are summarized in Table 2.

The as-prepared 3D C/C-SiC composite presents a bulk density of $2.0\text{--}2.1 \text{ g cm}^{-3}$ and a comparatively low open porosity in the range of 5–10%. In addition, the 3D C/C-SiC composite shows a

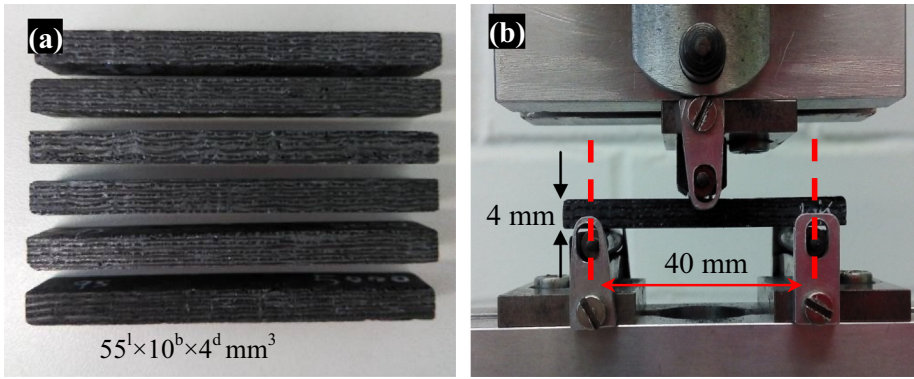


Fig. 2. Photographs of the 3 point flexural test (a) The specimens for 3 point flexural tests; (b) the setup for 3 point flexural/flexural fatigue tests. (For interpretation of the references to color in this figure legend, the reader is referred to the web version of this article.)

Table 1

The preselected parameters of fatigue tests for 3D C/C-SiC composites.

Series No.	Fatigue cycles	Flexural fatigue stresses (MPa)				
"Set 1"	$\leq 5 \times 10^4$	180–150	145	130	115	95
"Set 2"	2×10^3	130	115	95		
"Set 3"	20	95				
	2×10^3					
	5×10^3					
	1×10^4					
	5×10^4					

Table 2

The basic data of the as-prepared 3D C/C-SiC composites.

Sample	Bulk density/gcm ⁻³	Open porosity/%	3 point flexural strength /MPa	Flexural modulus/GPa	Number of tested samples
C/C-SiC	2.0–2.1	5–10	169 (23)	22.3 (1.8)	N = 19

Standard deviations are given in parentheses.

mean flexural strength of 169 MPa with a standard deviation of 23, by following the normal distribution.

It is well established that the strength of brittle materials follows the Weibull distribution. Regarding CMCs, the two basic constituents (fiber and matrix) are essentially brittle and the failure of the composite involves defect-induced randomly cracking [37]. Hence, the statistical distribution for the flexural strength of C/C-SiC composites in this work could be described by using the Weibull equation (3.1) [38].

$$F(\sigma) = 1 - \exp \left[-\left(\frac{\sigma}{\sigma_u} \right)^m \right] \quad (3.1)$$

where $F(\sigma)$ is the probability of failure, σ is the applied stress, σ_u is the characteristic strength, and m is the Weibull modulus. Generally, the Weibull modulus ' m ' indicates the scatter of the strength. A higher modulus means uniformity in strength resp. a higher reliability.

Fig. 3 displays the Weibull distribution for the quasi-static flexural strength. The Weibull modulus ' m ' is of 8.418 and the characteristic flexural strength is 178 MPa. As it can be seen in Fig. 3, the fitted line traces the data point with favorable accuracy. Therefore, it can be concluded that the Weibull distribution is appropriate to describe the failure distribution of the given composite. It should also be noted that the ' m ' for the flexural strength in this work is very close to the corresponding value (about 10) for the LSI based C/C-SiC composites in the Ref. [39].

Nevertheless, hereinafter it was preferred to apply the normal distribution to characterize the post-fatigue samples. Since it is required a high amount of samples to describe the Weibull distri-

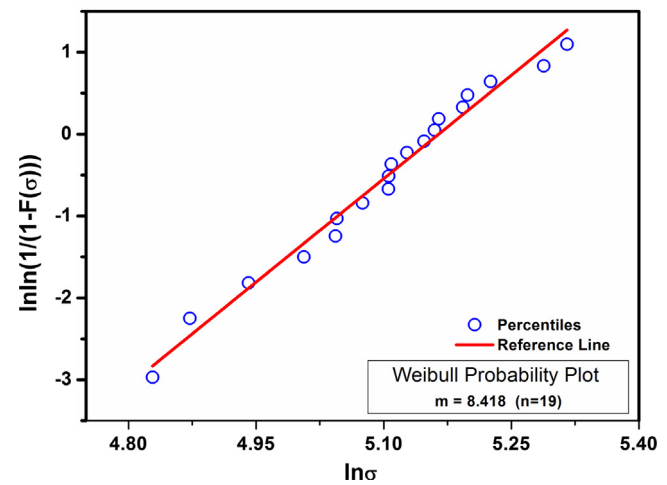


Fig. 3. The Weibull distribution for the quasi-static flexural strength. n in the parenthesis indicates the number of tested samples. (For interpretation of the references to color in this figure legend, the reader is referred to the web version of this article.)

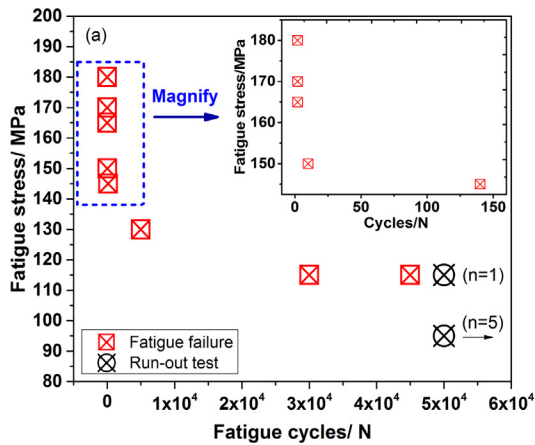
bution, it was not feasible to perform such analysis after several different fatigue loadings. However, it should be highlighted that given the high production costs of CMCs, and therefore the limited amount of testing material, it is generally accepted to characterize them using the normal distribution.

3.2. Behavior under fatigue loadings

Fig. 4(a) shows the diagram of flexural stress versus cycles to failure (S-N curve) for the 3D C/C-SiC composites. Obviously, the as-prepared C/C-SiC specimens survive the run-out of 5×10^4 cycles when the maximum fatigue stresses are lower than 115 MPa. Note that all tested samples exhibit a run-out after the desired 5×10^4 cycles when the applied fatigue stress decreases to 95 MPa. Moreover, it was observed that the cyclical overloaded stresses, especially when they are higher than 145 MPa, could break the specimens immediately or merely after a merely few fatigue cycles. In order to characterize the damage evolution under these stresses, a typical stress-strain diagram of a sample, which was subjected to the maximum fatigue stress of 145 MPa, is presented in **Fig. 4(b)**. During the first loading, a linear elastic behavior indicated by a constant elastic modulus is initially observed. Then the slope of the curve tends to decrease with the gradually increased loads until the maximum fatigue stress is achieved, indicating the generation of new damage in the composite. During the first unloading, a certain amount of permanent strain (PS) is measured. This indicates that the cracks, generated during the first loading, are not completely closed and fibers are not able to move to their original places during the unloading. Fracture mechanisms, including the matrix cracking, fiber/matrix debonding, delamination, interfacial frictions and fiber breakage could be introduced into the CMC during the fatigue loading, and results in the permanent strain observed after unloading [40,41]. The subsequent PS gradually increases and stress-strain loops start to overlap with each other until approximately 134 cycles. After this point, the stress-strain loops start to diverge (see the loops from 134th cycle to 140th cycle in **Fig. 4(b)**, probably because of the accumulation of damage, e.g. the increased amount of ruptured fibers. This is an indicative of that the reinforcements survived the first 134 cycles are no longer capable to carry the fatigue loads. Consequently, the 3D C/C-SiC specimen fails after merely 141 cycles.

3.3. Dependence of post-fatigue behavior on the previously applied stress

Based on the investigation as shown in **Fig. 4**, fatigue tests with maximum stress of 95 MPa, 110 MPa and 130 MPa and only 2000 cycles, were performed in order to investigate the stress-dependence of the RFS, within the framework of Set 2. Note that the specimens tested with the above-mentioned conditions are



not expected to fail during the fatigue loading. During a fatigue cycle, it is generally known, that the permanent strain can be related to the applied stress. Higher fatigue stresses result in more damage, corresponding to higher values of PS. As presented in **Fig. 5(a)**, the measured PS after 2000 cycles trends to increase with the increasing applied stress, despite the considerable margin of test error. Such standard deviations in permanent strain and quasi-static strength for C/C-SiC composites in this work derive from the highly inhomogeneous microstructures. In general, the distribution of phases, defects like pores and cracks, and fiber architecture (higher fiber volume fraction in the needled region) in the C/C-SiC composites is definitely uneven. Additionally, during LSI process the different damage in carbon fibers due to various protections from non-uniform PyC could also give rise to high standard deviations in mechanical properties of C/C-SiC composites.

The influence of different fatigue loadings on the RFS is displayed in **Fig. 5(b)**. Due to the fatigue stress induced damage as discussed above, the flexural modulus of the post-fatigue specimens, without doubt, gradually decreases to 17.8 GPa, around 80% of the as-processed modulus, when the maximum fatigue stress of 130 MPa is applied. However, it is noteworthy that the post-fatigue specimens show an increase RFS with higher applied fatigue loads in comparison to the as-prepared specimens. In other words, the RFS for C/C-SiC composites, to a certain extent, could be enhanced by the previous fatigue damage. Such strength enhancement on some of CMCs after cyclic loadings has also been proved in Refs. [32,42]. The stress-strain curves of the tested C/C-SiC specimens are shown in **Fig. 5(c)**. Compared to the as-prepared specimens, the post-fatigue specimens present a smaller portion of non-linearity in the stress-strain curve. Note that this linear-elastic response is derived from the fatigue-induced damage, and is also consistent with previous investigations on LSI based C/C-SiC composites subjected to cyclically tensile stress [26,43]. However, the “pseudo-plastic” fractured mode of the C/C-SiC composites under flexural loading remains after the fatigue loads. Therefore, it can be concluded that the crack-deflection mechanisms are still effective after the C/C-SiC specimens had undergone fatigue damage.

3.4. Dependence of the RFS on the applied cycles

Fig. 6(a) shows the typical flexural stress-strain loops of the specimen loaded with the maximum stress of 95 MPa. It was found that the specimen shows almost only elastic deformation during the first loading, corresponding to the linear stress-strain behavior.

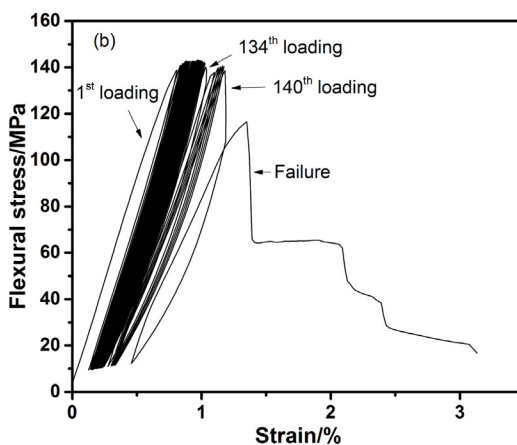


Fig. 4. (a) Diagram of the flexural stress vs. cycles to failure (S-N curve) for the 3D C/C-SiC composites at room temperature. n in the parenthesis indicates the number of samples achieved the run-out of 5×10^4 cycles. (b) The typical fatigue stress-strain loops of a specimen loaded with the maximum fatigue stress of 145 MPa. (For interpretation of the references to color in this figure legend, the reader is referred to the web version of this article.)

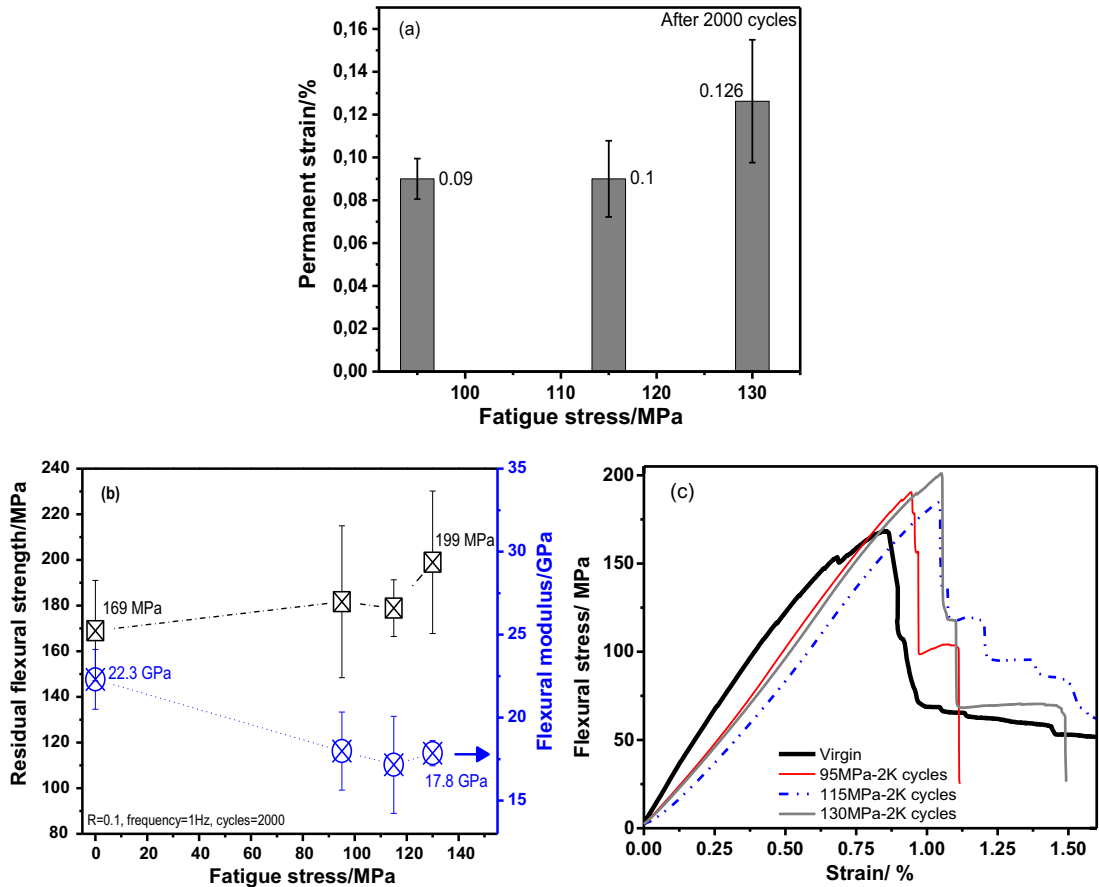


Fig. 5. (a) Diagram of maximum fatigue stress vs. permanent strain for the 3D C/C-SiC composites after 2000 cycles. (b) Diagram of the RFS/flexural modulus vs. applied fatigue stress. (c) Representative stress-strain curves of virgin and post-fatigue specimens. (For interpretation of the references to color in this figure legend, the reader is referred to the web version of this article.)

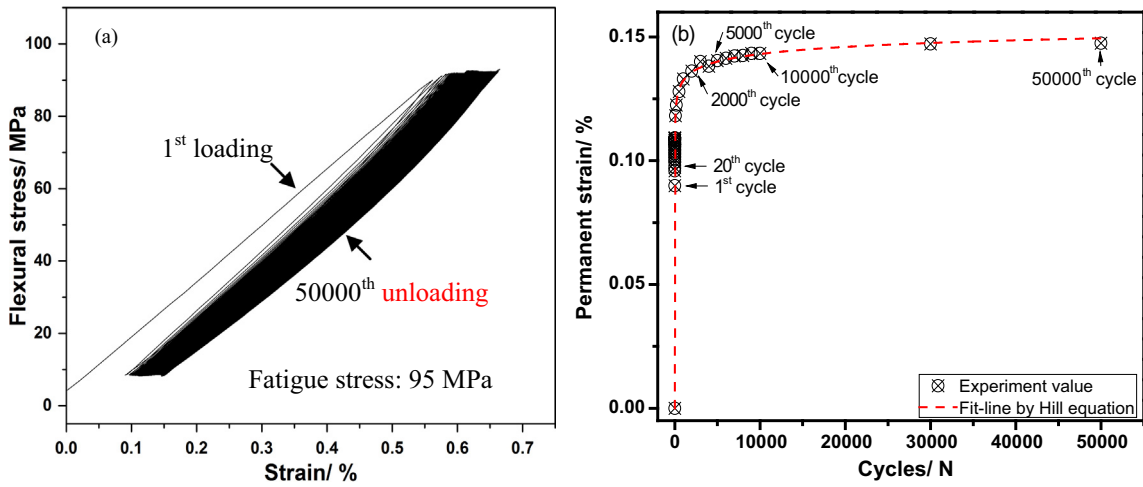


Fig. 6. (a) Typical flexural stress-strain loops of the specimen loaded with the maximum fatigue stress of 95 MPa; (b) Permanent strain vs. number of applied cycles with the maximum stress of 95 MPa. (For interpretation of the references to color in this figure legend, the reader is referred to the web version of this article.)

In addition, the PS was measured after the first loading cycles, which is identical to the mechanical response of the specimen subjected to the fatigue stress of 145 MPa (see Fig. 4(b)). Thereafter, the hysteresis loops progressively overlap from the 2nd to 50,000th cycle, indicating a gradual increment of the fatigue damage. Note that PS in Fig. 6(a) spans a strain range of approximately 0.05% while maximum-stress strain spans double of that, 0.1%.

Such difference in the width of strain range is probably ascribed to the change of thermal residual stress in the lower part of the specimen during loading/unloading. The cyclic tensile stress derived from the cyclic flexural loads will gradually relieve the compressive TRS in the 90° fiber bundles during loading, resulting in wider strain-range than PS during unloading. The similar phe-

nomena in the strain-range caused by TRS were particularly evident in the step-loading curves from Mei and Dassios, etc. [18,44].

In addition, differently than the sample tested with maximum fatigue stress of 145 MPa, the well overlapped loops also demonstrate that the cracking in the C/C-SiC composites is probably saturated until the specimen tested with 95 MPa reaches the run-out.

Fig. 6(b) presents the evolution of PS when the maximum fatigue stress of 95 MPa is applied. The data points could be well fitted, $R^2 = 0.999$, by the Hill equation (3.2) as follows.

$$PS = 0.17869X^{0.1495} / (0.9106^{0.1495} + X^{0.1495}) \quad (3.2)$$

where X is the number of cycles.

Moreover, the growth rate of PS, namely the slope of the PS, as a function of fatigue cycles X can be calculated by the first order derivative of Eq. (3.2) and is expressed as:

$$y = 0.0263 / (X^{0.1495} + 1.9722X + 0.9724X^{0.8505}) \quad (3.3)$$

where y is the growth rate of PS.

It is visible that the growth rate of PS is decreasing with the increased cycles, which indicates that less and less new damage could be introduced into the composites with the higher fatigue period. Whereas the total amount of damage are still increasing with cycles.

According to previous investigations [16,45], it is proposed that the length of the cyclic loading period exerts a profound influence on the residual strength of CMCs. Based on the different growth rates of PS during the above fatigue loading, five kind of representative damages, corresponding to $20, 2 \times 10^3, 5 \times 10^3, 1 \times 10^4$ and 5×10^4 cycles under the fatigue stress of 95 MPa, were introduced into the 3D C/C-SiC specimens to study the cycle-dependence of the RFS, as listed in Set 3.

Fig. 7(a) displays the diagram of the RFS/flexural modulus versus fatigue cycles under the maximum fatigue stress of 95 MPa. It can be perceived that the flexural modulus gradually decrease with the increasing number of fatigue cycles, which coincides with the increment of PS as shown in **Fig. 6(b)**. It is well established that higher PS value indicates more fatigue-induced damages, which leads to lower modulus. This is also in accordance to the results obtained with different applied fatigue stresses, cf. **Fig. 5(a)**. Nevertheless, the RFS of the fatigued specimens, as shown in **Fig. 7(a)**, increase after 20, 2000, 5000 and 10,000 cycles. In this work, the most pronounced enhancement induced by fatigue damage on RFS (about 110% of the virgin strength) is measured in the post-fatigue specimens after merely 5000 loading cycles. The increased RFS after fatigue loadings reconfirms the existence of strength enhancement behavior in CMC, even subjected to flexural loadings as described in the Ref. [32]. However the RFS tends to decrease when the number of the cycle exceeds 5000. Note that the RFS after 50,000 fatigue cycles declines to approximately 156.3 MPa, corresponding to 92.5% of the flexural strength in the virgin specimens. It is likely that the RFS will further decrease with the increasing loading cycles.

Fig. 7(b) presents the representative stress-strain curves of the specimens loaded for different fatigue cycles. Again it is noticeable that a reduction of the non-linear region in stress-strain curves is observed in the post-fatigue specimens. Still, the “pseudo-plastic” fractured mode is presented in all specimens.

In conclusion, when the 3D C/C-SiC composite specimens are exposed to cyclic flexural loads, the RFS and flexural modulus depend on the number of cycles or the applied fatigue stresses. On the basis of above-mentioned results, it can be concluded that a suitable fatigue loading could enhance the RTS of the 3D C/C-SiC composite with the expense of its flexural modulus, and part of its non-linear behavior. Nonetheless, the fatigue damage in this work hardly seems to influence the crack-deflection mechanisms in a

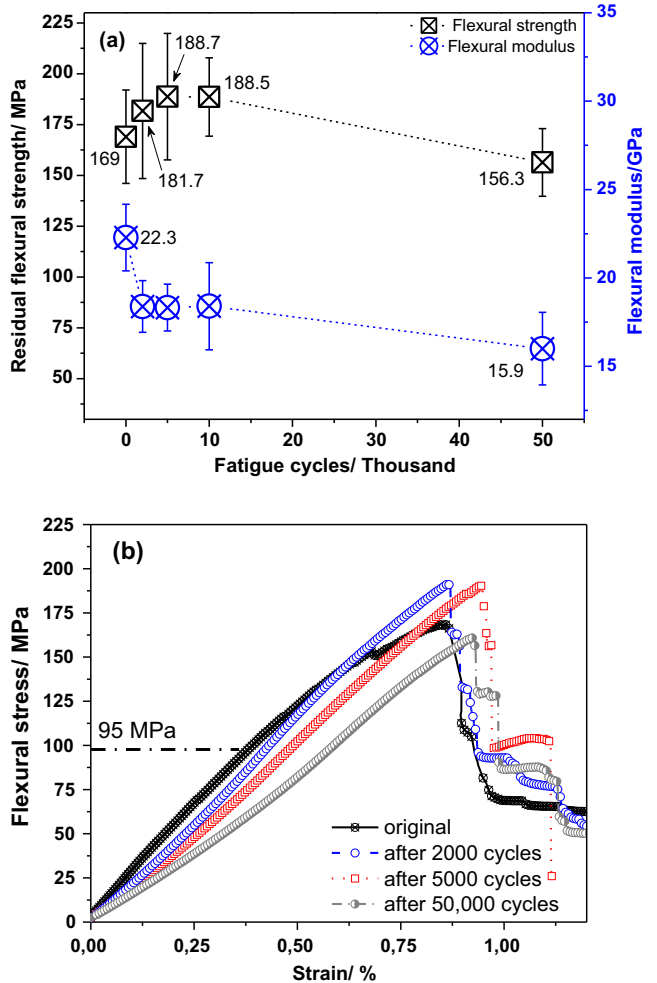


Fig. 7. (a) Diagram of the RFS/flexural modulus vs. fatigue cycles for samples tested with fatigue stress of 95 MPa. (b) Representative stress-strain curves of virgin and post-fatigue specimens. (For interpretation of the references to color in this figure legend, the reader is referred to the web version of this article.)

significant matter. However, the excessive fatigue with overloaded stresses (see **Fig. 5(b)**) or too long periods (see **Fig. 7(b)**) will be undoubtedly detrimental to the strength and post-fatigue behavior of the composite, or even cause the premature failure for the C/C-SiC composites.

3.5. Microstructures

Fig. 8 shows the typical microstructures of 3D C/C-SiC specimens before and after cyclical loadings. Even before any flexural loading, the microstructure of virgin specimen reveals several small cracks in different directions, as shown in **Fig. 8(a)**. These cracks can be related to process-induced defects due to the mismatch of the thermal expansion coefficient between the fibers and the matrix. Note that most of the cracks in the virgin specimens are orientated vertically to the 90° fiber bundles because of the tensile residual stress in 0° fiber bundles and chopped-fiber web layers. More details about these thermal residual stresses in 3D C/C-SiC composites have been reported in our previous work [26].

Fig. 8(b) presents the microstructure of loaded region for the post fatigue specimen (95 MPa, 50,000 cycles). The cracks propagate rather straight from the bottom surface and across the 0° fiber bundles, chopped fiber cloth layers and 90° fiber bundles could be

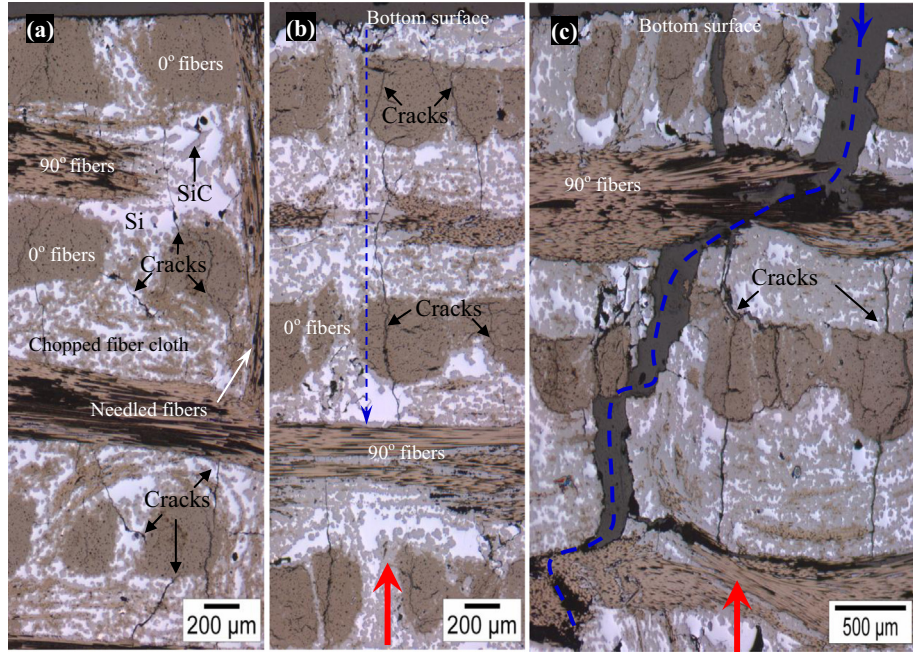


Fig. 8. Typical microstructures of 3D C/C-SiC before/after cyclical loading. (a) Virgin specimen without fatigue loading. (b) Loaded region of the specimen that survived 5×10^4 cycles with the fatigue stress of 95 MPa. (c) Quasi-static fracture of the specimen that underwent 5×10^4 cycles with fatigue stress of 95 MPa. Red arrows indicate the direction of bending load, while the blue dashed arrow indicates the path and direction of the crack propagation. (For interpretation of the references to color in this figure legend, the reader is referred to the web version of this article.)

observed. It can be assumed that the fatigue loading initiates/propagates the process-induced cracks leading to a crack front which is parallel to the applied load to the specimen. Within this assumption, it is expected that these cracks will open and close during loading and unloading, respectively. However, their propagations are stopped at the next 90° oriented fibers. This can be confirmed by the linear behavior of the stress-strain loops, and the reduction of PS growth rate, cf. Fig. 6. After the quasi-static loading until failure, the fatigue-induced cracks propagate further, as shown in Fig. 8(c). Crack propagating seems to go straight through the 0° fibers and short fiber cloth layers, while it deflects in the 90° fibers. Moreover, pull-out of 90° fibers is also observed on the bottom to the inner portion of the specimen. Most importantly, no apparent shear failure could be observed between the 90° fibers and others layers. Hence, the influence of shear stress between the fiber layers on the flexural strength could be negligible. Note that the specimens, in general, fail when the 90° fibers which are closest to the tensile loaded side of the specimen break. In other words, it could be concluded that the 90° fibers determine the mechanical behavior for the 3D C/C-SiC composites under flexural loadings in this work.

Fig. 9 shows the morphology of the fractured surfaces from virgin and post-fatigue specimens after quasi-static flexural tests. The fibers pull-out observed in the virgin specimens, as shown in Fig. 9(a) and (b), are mainly consisted of many fiber bundles and few single fibers. Additionally, it could be perceived that the forepart of the pull-out fiber bundles as shown in Fig. 9(b) are still intact, and most of the fibers are still embedded in the matrix, indicating the considerable strong bonding between fiber and matrix. Compared to the fiber-pullout pattern in virgin specimens, more single fibers could be observed in the post-fatigue specimens which were previously loaded for 10,000 cycles (see Fig. 9(c)). Note that there are still some fragments of matrix in these fiber clusters, but a lot less amount than that in the virgin specimens. As the fatigue damage progressively introduced, the fiber/matrix bonding will further degrade due to the interfacial sliding during the cyclic load-

ing/unloading. For this reason, the largest amount of single fibers could be observed in the specimen loaded for 50,000 cycles, as shown in Fig. 9(e). Furthermore, the single fibers with much smoother surfaces in the forepart of pull-out bundles (see Fig. 9(f)) markedly reaffirms the weakening of interfacial bonding in the C/C-SiC after loading for 50,000 cycles. Moreover, it is noteworthy that the fiber length after cyclic loading is seemingly longer than that of virgin specimens. Generally, the fiber-pullout length is inversely proportional to the interfacial shear strength (ISS). The ISS τ of CMCs can be described by Eq. (3.4) [46].

$$\tau = \frac{\sigma_f d}{2L_c} \quad (3.4)$$

where d is the fiber diameter, σ_f is the fiber strength, and L_c is the critical length of broken fiber which equal to twice of fiber pull-out length.

Hence, it can be inferred from Fig. 9 and Eq. (3.4) that the post fatigue specimens show somewhat lower ISS in comparison to that of virgin specimens.

3.6. Discussion

According to the experimental results mentioned above, the lifetime of the 3D C/C-SiC composite under fatigue loading is strongly dependent on the fatigue damage evolution during loading and unloading. According to the microstructure analysis, the damage induced by the cyclic stresses can be mainly described as crack propagation and interfacial degradation. However, before relating these two mechanisms with the observed behavior, it should be noted that the fatigue damage evolution does not occur evenly throughout the bending specimen. It is well known that the specimen for flexural test is subjected to a stress distribution along its thickness, which results in tensile stresses at the bottom, compressive stresses at the top, and a neutral plane in the middle, for an isotropic material. Since CMCs are rather heterogeneous, the stress distribution is definitely not the same as the theorized iso-

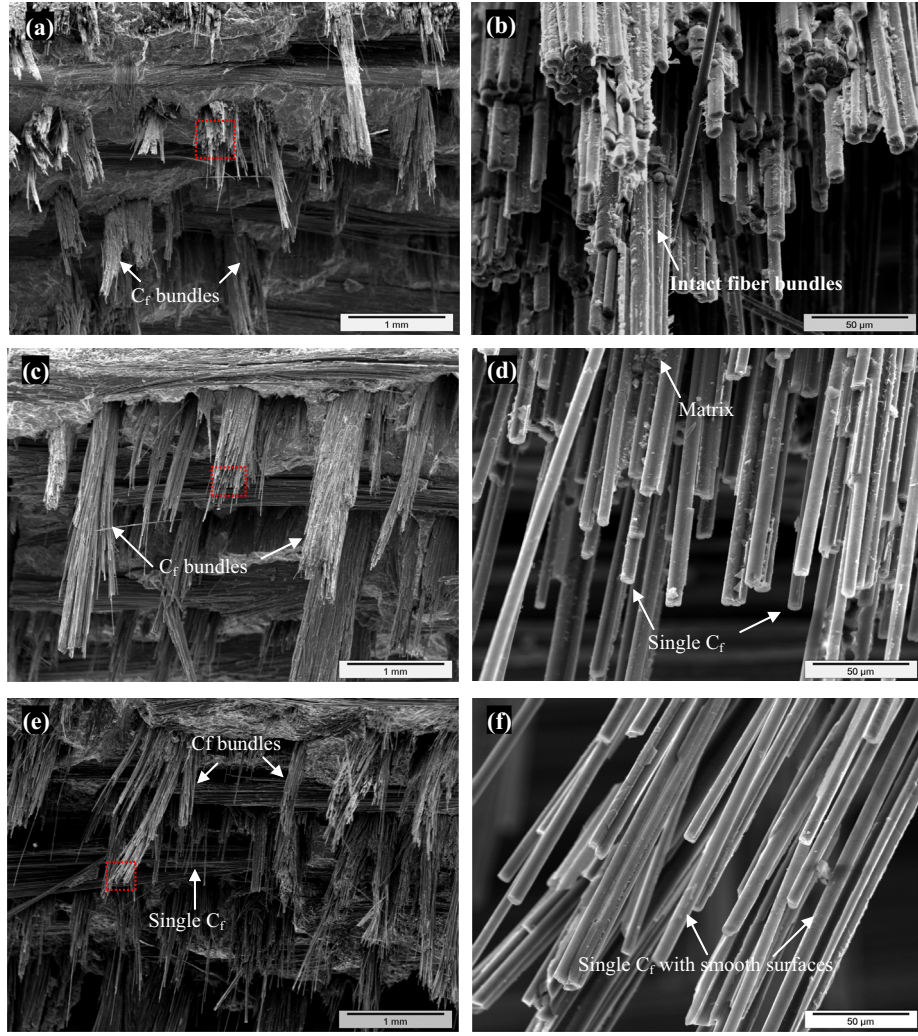


Fig. 9. Typical fracture surfaces of quasi-static flexural tests on 3D C/C-SiC without/after previous cyclical loadings. (a) Virgin specimen; (b) Magnification of the highlighted region in (a); (c) Specimen loaded with fatigue stress of 95 MPa for 1×10^4 cycles; (d) Magnification of the highlighted region in (c); (e) Specimen loaded with fatigue stress of 95 MPa for 5×10^4 cycles; (f) Magnification of the highlighted region in (e). (For interpretation of the references to color in this figure legend, the reader is referred to the web version of this article.)

tropic materials. However, the maximum tensile and compressive stresses are still located at the bottom and top of the sample, respectively, and somewhere in-between it is expected to be a neutral plane.

Given these considerations, it can be concluded that the generated damage during fatigue loading/unloading has a maximum in the bottom of the sample, see Fig. 8(b), and is less intense towards the neutral plane. Note that damage is also generated in the upper half of the sample, compressive zone, but it is presumably less critical than the lower half, tensile zone. In this matter, the resistance of the material will be given by the plies, *i.e.* the bottom 90° fiber bundles that can sustain the maximum tensile load. For moderate fatigue stresses, *e.g.* 95 MPa, crack propagation starts in the bottom plies, but is not strong enough to break the 90° fibers. Therefore, the fatigue damage tends to get saturated. Consequently, there is a drastic reduction of the PS growth rate at around 2000 cycles, cf. Fig. 6(b). If the fatigue stress is high enough, for instance 145 MPa, the continuous cracking in the lower part will eventually lead to the failure of the bottom 90° fibers. At this point, the C/C-SiC specimen will no longer be able to undertake the load, and will progressively fail, shown in Fig. 4(b).

The mechanical properties of the post-fatigue specimen will also be dependent on the fatigue induced damage. As seen in the

experimental results, the residual flexural strength increases up to an extent due to the crack propagation and interfacial degradation. Regarding the cracking, previous studies show that it could result in enhanced strength by relieving the thermal residual stresses [46]. Interfacial friction can also play an important role in the post-fatigue mechanical behavior since it weakens the fiber/matrix interface. As discussed in Ref. [47], the fiber/matrix interface is one of the most predominant factors to determine the strength of CMCs. On the basis of the microstructure, it could be concluded that the interfacial degradation of the 90° fibers could lead to crack deflection along the fibers and then result in higher residual flexural strength. However, it should be noted that the extent of both mechanism described above is mainly localized on the lower part of the specimen. In the lower part, the generation of defects leads to a decreased flexural modulus and partial loss of the non-linear behavior. Moreover, if the amount of damage is too high, after 50,000 cycles for instance, there will be probably stress concentrations at the lower 90° fibers. Additionally, the detrimental effect caused by interfacial debonding, *e.g.* fiber wear under cyclic loading/unloading is more pronounced to result in weakened strength. As a consequence, a decrease of strength was measured as seen in Fig. 7(a). However, since the damage is more localized at the bottom layers, the upper part of the composite can still properly

deflect cracks. Therefore, even those post-fatigue samples show quasi-plastic failures.

4. Conclusions

The influence of quasi-static and cyclic flexural loadings with different stress levels and cycles on the mechanical behavior of a 3D C/C-SiC composites were here studied. Based on the performed investigations, following conclusions could be drawn:

- (a) The Weibull modulus and flexural characteristic strength of the 3D C/C-SiC composites were 8.418 and 178 MPa, respectively. However, due to the low amount of samples, the normal distribution was used to evaluate the RFS, and the mean flexural strength of 169 ± 23 MPa was used as reference.
- (b) The fatigue limit, considering a run-out of 5×10^4 cycles, was found to be at 95 MPa (56% of the mean flexural strength).
- (c) The cyclic tensile loads in the lower part of the specimen result in strength enhancement with the expense of decreased flexural modulus due to the fatigue damage, for instance cracking and interfacial degradation after short fatigue duration. The post fatigue specimens with the maximum stress of 130 MPa for 2000 cycles could achieve the RFS of 199 MPa (117% of the mean flexural strength).
- (d) The RFS showed dependence on the number of applied fatigue cycles and stress level, because the damage in 90° fiber plies at the lower part of the specimen under cyclic tensile loadings basically determined the ultimate flexural strength.
- (e) The upper part of the specimens, which is almost free of fatigue damage under cyclic compressive loadings, can still properly deflect cracks and result in quasi-plastic failures like virgin specimens.
- (f) Based on the microstructure investigation, the interfacial degradation and crack propagation after short fatigue duration, which occur mostly on the lower part of the specimen, determined the stress-induced enhancement of the flexural strength. Whereas the specimens will suffer lose in strength rapidly, after 50,000 cycles for instance, because of the considerable stress concentrations and fibers wear at 90° fiber bundles in the lower part.

Acknowledgement

The authors gratefully acknowledge the financial supports from the National Natural Science Foundation of China (Grant No. 51575536), Natural Science Foundation of Hunan Province (Grant No. 2015JJ3163), Science and Technology Planning Project of Hunan Province (Grant No. 2015RS4016). Additionally, the authors would like to express the heartfelt gratitude to Dr. Jiang Shao-hua, Mr. Walter Müller from University of Bayreuth in Germany and Mr. Lu Yu-hai from Central South University in China for their kind assistances during the preparation of this manuscript.

References

- [1] Krenkel W, Schanz P. Fiber ceramic structures based on liquid impregnation technique. *Acta Astronaut* 1992;28:159–69.
- [2] Krenkel W. Carbon fiber reinforced CMC for high-performance structures. *Int J Appl Ceram Technol* 2004;1:188–200.
- [3] Reichert F, Langhof N, Krenkel W. Influence of thermal fiber pretreatment on microstructure and mechanical properties of C/C-SiC with thermoplastic polymer-derived matrices. *Adv Eng Mater* 2015;17:1119–26.
- [4] Xiao P, Li Z, Xiong X. Microstructure and tribological properties of 3D needle-punched C/C-SiC brake composites. *Solid State Sci* 2010;12:617–23.
- [5] Abu El-Hija H, Krenkel W, Hugel S. Development of C/C-SiC brake pads for high-performance elevators. *Int J Appl Ceram Technol* 2005;2:105–13.
- [6] Krenkel W, Berndt F. C/C-SiC composites for space applications and advanced friction systems. *Mater Sci Eng A* 2005;412:177–81.
- [7] Li Z, Xiao P, Zhang B-G, Li Y, Lu Y-H, Zhu S-H. Preparation and dynamometer tests of 3D needle-punched C/C-SiC composites for high-speed and heavy-duty brake systems. *Int J Appl Ceram Technol* 2016;13:423–33.
- [8] Li Z, Long Y, Li Y, Li J-W, Xiong X, Xiao P. Microstructure and properties of needle punching chopped carbon fiber reinforced carbon and silicon carbide dual matrix composite. *Ceram Int* 2016;42:9527–37.
- [9] Li Z, Xiao P, Xiong X, Huang B-Y. Preparation and tribological properties of C fibre reinforced C/SiC dual matrix composites fabrication by liquid silicon infiltration. *Solid State Sci* 2013;16:6–12.
- [10] Fan S, Zhang L, Xu Y, Cheng L, Lou J, Zhang J, et al. Microstructure and properties of 3D needle-punched carbon/silicon carbide brake materials. *Compos Sci Technol* 2007;67:2390–8.
- [11] Fan S, Zhang L, Cheng L, Yang S. Microstructure and frictional properties of C/SiC brake materials with sandwich structure. *Ceram Int* 2011;37:2829–35.
- [12] Wang Y, Wu H. Microstructure of friction surface developed on carbon fibre reinforced carbon-silicon carbide (Cf/C-SiC). *J Eur Ceram Soc* 2012;32:3509–19.
- [13] Wang Y, Wu H. Friction surface evolution of carbon fibre reinforced carbon/silicon carbide (Cf/C-SiC) composites. *J Eur Ceram Soc* 2010;30:3187–201.
- [14] Li Z, Liu Y-Z, Zhang B-G, Lu Y-H, Li Y, Xiao P. Microstructure and tribological characteristics of needled C/C-SiC brake composites fabricated by simultaneous infiltration of molten Si and Cu. *Tribol Int* 2016;93:220–8.
- [15] Li Z, Xiao P, Zhang B-G, Li Y, Lu Y-H. Preparation and tribological properties of C/C-SiC brake composites modified by in situ grown carbon nanofibers. *Ceram Int* 2015;41:11733–40.
- [16] Sørensen BF, Holmes JW, Vanswijghoven EL. Rate of strength decrease of fiber-reinforced ceramic-matrix composites during fatigue. *J Am Ceram Soc* 2000;83:1469–75.
- [17] Mei H, Cheng L. Stress-dependence and time-dependence of the post-fatigue tensile behavior of carbon fiber reinforced SiC matrix composites. *Compos Sci Technol* 2011;71:1404–9.
- [18] Dassios KG, Aggelis DG, Kordatos EZ, Matikas TE. Cyclic loading of a SiC-fiber reinforced ceramic matrix composite reveals damage mechanisms and thermal residual stress state. *Compos A Appl Sci Manuf* 2013;44:105–13.
- [19] Sørensen BF, Holmes JW, Vanswijghoven EL. Does a true fatigue limit exist for continuous fiber-reinforced ceramic matrix composites? *J Am Ceram Soc* 2002;85:359–65.
- [20] Chawla N, Tur YK, Holmes JW, Barber JR, Szweda A. High-frequency fatigue behavior of woven-fiber-fabric-reinforced polymer-derived ceramic-matrix composites. *J Am Ceram Soc* 1998;81:1221–30.
- [21] Holmes JW, Wu X, Sørensen BF. Frequency dependence of fatigue life and internal heating of a fiber-reinforced/ceramic-matrix composite. *J Am Ceram Soc* 1994;77:3284–6.
- [22] Fantozzi G, Reynaud P. Mechanical hysteresis in ceramic matrix composites. *Mater Sci Eng, A* 2009;521:522:18–23.
- [23] Goto K, Hatta H, Katsu D, Machida T. Tensile fatigue of a laminated carbon-carbon composite at room temperature. *Carbon* 2003;41:1249–55.
- [24] Kordatos EZ, Dassios KG, Aggelis DG, Matikas TE. Rapid evaluation of the fatigue limit in composites using infrared lock-in thermography and acoustic emission. *Mech Res Commun* 2013;54:14–20.
- [25] Zhang Y, Cheng L, Zhang L, Luan X. Comparative analysis of low-cycle fatigue behavior of 2D-Cf-PyC/SiC composites in different environments. *Int J Appl Ceram Technol* 2015;12:491–9.
- [26] Li Y, Xiao P, Luo H, Almeida RSM, Li Z, Zhou W, et al. Fatigue behavior and residual strength evolution of 2.5D C/C-SiC composites. *J Eur Ceram Soc* 2016;36:3977–85.
- [27] Belingardi G, Cavatorta M. Bending fatigue stiffness and strength degradation in carbon-glass/epoxy hybrid laminates: cross-ply vs. angle-ply specimens. *Int J Fatigue* 2006;28:815–25.
- [28] Van Paepengem W, Degrieck J. Experimental set-up for and numerical modelling of bending fatigue experiments on plain woven glass/epoxy composites. *Compos Struct* 2001;51:1–8.
- [29] Capela C, Ferreira JAM, Febra T, Costa JD. Fatigue strength of tubular carbon fibre composites under bending/torsion loading. *Int J Fatigue* 2015;70:216–22.
- [30] Yang X, Li H-J, Yu K-H, Zhang S-Y. Effect of stress level on fatigue behavior of 2D C/C composites. *Trans Nonferr Metals Soc China* 2013;23:2135–40.
- [31] Tanabe Y, Yoshimura T, Watanabe T, Hiraoka T, Ogita Y, Yasuda E. Fatigue of C/C composites in bending and in shear modes. *Carbon* 2004;42:1665–70.
- [32] Xue L-Z, Li K-Z, Jia Y, Zhang S-Y, Cheng J, Guo J. Flexural fatigue behavior of 2D cross-ply carbon/carbon composites at room temperature. *Mater Sci Eng A* 2015;634:209–14.
- [33] Lu X-F, Xiao P. Preparation of in situ grown silicon carbide nanofibers radially onto carbon fibers and their effects on the microstructure and flexural properties of carbon/carbon composites. *Carbon* 2013;59:176–83.
- [34] Xiao P, Lu X-F, Liu Y, He L. Effect of in situ grown carbon nanotubes on the structure and mechanical properties of unidirectional carbon/carbon composites. *Mater Sci Eng A* 2011;528:3056–61.
- [35] Fan X, Yin X, Chen L, Zhang L, Cheng L. Mechanical behavior and electromagnetic interference shielding properties of C/SiC-Ti₃Si(Al)₂. *J Am Ceram Soc* 2016;99:1717–24.
- [36] Liao X, Li H, Xu W, Li K. Effects of tensile fatigue loads on flexural behavior of 3D braided C/C composites. *Compos Sci Technol* 2008;68:333–6.
- [37] Xu Y, Cheng L, Zhang L, Yin H, Yin X. Mechanical properties of 3D fiber reinforced C/SiC composites. *Mater Sci Eng A* 2001;300:196–202.

- [38] Suresh K, Sweety K, Anil K, Anupam S, Gupta AK, Rohini Devi G. Mechanical properties of LSI based 3D-stitched-C-SiC composites prepared by coal-tar pitch as carbon precursor. *Scripta Mater* 2008;58:826–9.
- [39] Kumar S, Kumari S, Kumar A, Shukla A, Devi GR, Gupta AK. Investigation of effect of siliconization conditions on mechanical properties of 3D-stitched C-SiC composites. *Mater Sci Eng, A* 2011;528:1016–22.
- [40] Liu C, Cheng L, Luan X, Li B, Zhou J. Damage evolution and real-time non-destructive evaluation of 2D carbon-fiber/SiC-matrix composites under fatigue loading. *Mater Lett* 2008;62:3922–4.
- [41] Goto K, Furukawa Y, Hatta H, Kogo Y. Fatigue behavior of 2D laminate C/C composites at room temperature. *Compos Sci Technol* 2005;65:1044–51.
- [42] Fang G, Gao X, Yu G, Zhang S, Chen J, Song Y. Effect of the stress level on the fatigue strengthening behavior of 2D needled C/SiC CMCs at room temperature. *Mater Des* 2016;89:432–8.
- [43] Li Y, Xiao P, Li Z, Zhou W, Liensdorf T, Freudenberg W, et al. Tensile fatigue behavior of plain-weave reinforced Cf/C-SiC composites. *Ceram Int* 2016;42:6850–7.
- [44] Mei H. Measurement and calculation of thermal residual stress in fiber reinforced ceramic matrix composites. *Compos Sci Technol* 2008;68:3285–92.
- [45] Li Y, Xiao P, Li Z, Zhou W, Liensdorf T, Freudenberg W, et al. Strength evolution of cyclic loaded LSI-based C/C-SiC composites. *Ceram Int* 2016;42:14505–10.
- [46] Mizuno M, Zhu S, Nagano Y, Sakaida Y, Kagawa Y, Watanabe M. Cyclic-fatigue behavior of SiC/SiC composites at room and high temperatures. *J Am Ceram Soc* 1996;79:3065–77.
- [47] Koch D, Tushev K, Grathwohl G. Ceramic fiber composites: experimental analysis and modeling of mechanical properties. *Compos Sci Technol* 2008;68:1165–72.